Journal of Alloys and Compounds 515 (2012) 166–170

Contents lists available at SciVerse ScienceDirect

Journal of Alloys and Compounds

journal homepage: www.elsevier.com/locate/jallcom

Structural and piezoelectric characteristics of BNT–$BT_{0.05}$ thin films processed by sol–gel technique

Marin Cernea [a,*], Lucian Trupina [a], Cristina Dragoi [a], Bogdan S. Vasile [b], Roxana Trusca [c]

[a] National Institute of Materials Physics, P.O. Box MG-7, Bucharest, Magurele 077125, Romania
[b] University POLITEHNICA of Bucharest, 060042, Romania
[c] METAV-R&D S.A., P.O. 22, Bucharest, Romania

ARTICLE INFO

Article history:
Received 14 September 2011
Received in revised form
23 November 2011
Accepted 26 November 2011
Available online 6 December 2011

Keywords:
$(Bi_{0.5}Na_{0.5})_{0.95}Ba_{0.05}TiO_3$ thin films
Sol–gel processes
Piezoelectric properties

ABSTRACT

Polycrystalline ferroelectric lead-free $(Bi_{0.5}Na_{0.5})_{0.95}Ba_{0.05}TiO_3$ (BNT–$NT_{0.05}$) thin films have been deposited on $Pt/TiO_2/SiO_2/Si$ substrates by an optimized sol–gel/spin-coating process. The film thermal treated at 700 °C is dense and well crystallized in the rhombohedral perovskite phase. The film is composed of polyhedral shaped primary particles with an average size of approximately 35 nm, and has a smooth surface of 4.52 nm root mean square roughness (RMS). The nanoscale electrical properties of the film were investigated by piezoforce microscopy (PFM). The PFM data showed that most of the grains seem to be constituted of ferroelectric multiple domains. The maximum dielectric constant measured at zero bias voltage is about 210 and the leakage current density has a value of about 3×10^{-5} A/cm^2 at an applied voltage about 8 V. These results indicate that, the BNT–$NT_{0.05}$ thin film is a promising functional lead-free ferroelectric material.

© 2011 Elsevier B.V. All rights reserved.

1. Introduction

Recently, bismuth sodium titanate $Bi_{0.5}Na_{0.5}TiO_3$ (abbreviated as BNT) and its solid solutions $(1-x)(Bi_{0.5}Na_{0.5})TiO_3$–$x$$BaTiO_3$, (BNT–$BT_x$) are intensively studied as lead-free piezoelectric materials [1–9]. The BNT–BT_x solid solutions with a composition near rhombohedral–tetragonal morphotropic phase boundary (MPB, x = 0.06–0.07) has attracted considerable attention due to their high piezoelectric properties [10–13]. The ceramics of BNT–BT_x are focused on the ferroelectric, dielectric and piezoelectric properties [11–14], while the BNT–BT_x thin films are only focused on the ferroelectric and dielectric properties [15–17]. Piezoelectric materials, especially in form of thin films, offer a number of advantages in MEMS, such as low hysteresis, high available energy density, high sensitivity with wide dynamic range, and low power requirement [18]. The sol–gel method is one of the most widely used to produce high quality coatings [19–22]. The sol–gel technique can produce thin bond-coating in order to provide excellent adhesion between the metallic substrate and the top coat [23]. There is very scarce literature about BNT thin films [24–27] and BNT–BT_x thin films [16,23,28] prepared by sol–gel/spin-coating. In this paper, we report on the uniformity and quality of the solution coatings, the phase composition of the crystalline films, the microstructure, and dielectric, ferroelectric and piezoelectric properties of BNT–$BT_{0.05}$ thin films derived from sol–gel. The potentiality of these lead-free films for microelectronic applications is discussed here.

2. Experimental procedures

Precursor sol of $0.95[(Bi_{0.5}Na_{0.5})TiO_3]$–$0.05[BaTiO_3]$ was prepared by an acetate–alkoxide sol–gel technique. Anhydrous sodium acetate (CH_3COONa, 99.995%, Aldrich), barium acetate ($(CH_3COO)_2Ba$, 99%, Aldrich), bismuth(III) acetate ($(CH_3COO)_3Bi$, 99.99+%, Aldrich) and titanium(IV) isopropoxide, 97% solution in 2-propanol ($Ti\{OCH(CH_3)_2\}_4$, Aldrich), were used as starting chemical reagents. Acetic acid (≥99.7%, Aldrich) was used as solvent for the metallic acetates. The detailed sol–gel procedure was published elsewhere [29]. The films were deposited on Si/SiO_2 (450 nm)/TiO_2(15 nm)/Pt(100 nm) substrate by spin casting, at 3000 rpm for 20 s. Then, the gel-films were dried at 200 °C for 2 min in order to evaporate the solvent, and pyrolyzed at 400 °C for 4 min, in air, for organic components removal. The films were prepared by repeating (10 times) the deposition and pyrolysis cycle. The coated films were finally calcined in air at 700 °C, 1 h, for achieving crystallization.

The structure of the films was analyzed by a Bruker D8 Advance X-ray diffractometer. The microstructure of the samples was investigated using a FEI Quanta Inspect F scanning electron microscope (SEM) and, a Tecnai^{TM} G^2 F30 S-TWIN transmission electron microscope with a line resolution of 1 Å, in high-resolution transmission electron microscopy (HR-TEM) mode and selected area electron diffraction (SAED). An atomic force microscope (AFM) (Asylum MFP 3D SA, Asylum Research) was employed to obtain high resolution images of the surface and to determine the roughness and quality of the spin-coated films. Conductive Pt-coated silicon cantilevers (AC240-TM, Olympus, l = 240 μm, resonant frequency ∼70 kHz, spring constant = 2 N/m) were used for simultaneous acquisition of topographic views and domain imagining using a MFP-3D Piezo Force Module. DART (Dual AC Resonance Tracking) measurement technique was used for study of the local electromechanical activity at nanoscale size. The small displacement of the thin film induced by the converse piezoelectric effect was measured on the film surface without top electrodes, as a function of a dc switching bias superimposed on ac

* Corresponding author. Tel.: +40 21 369 01 70x130; fax: +40 21 369 01 77.
E-mail address: mcernea@infim.ro (M. Cernea).

0925-8388/$ – see front matter © 2011 Elsevier B.V. All rights reserved.
doi:10.1016/j.jallcom.2011.11.129

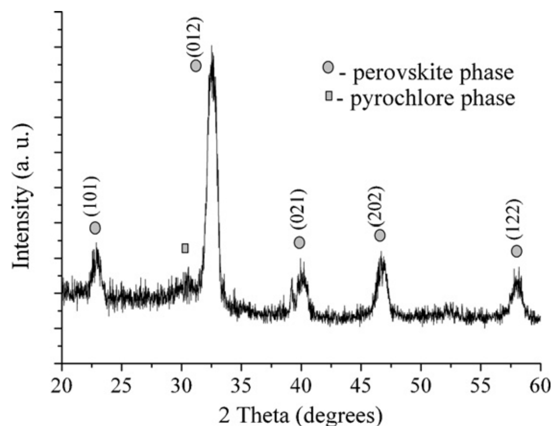

Fig. 1. XRD patterns of sol–gel/spin-coating processed BNT–$BT_{0.05}$ thin films.

modulation bias. The dielectric properties of BNT–$BT_{0.05}$ thin films were evaluated using a capacitor structure of Au/BNT–$BT_{0.08}$/Pt, where the Au top electrode was deposited by sputtering through a designed mask with dimensions of 0.2 mm^2 onto the film surfaces. The capacitance was measured with an Agilent LCR meter; for current measurements we used a Keithley 6517 electrometer, while the hysteresis was measured with a TF2000 ferroelectric tester.

3. Results and discussion

3.1. Structure

The XRD patterns (Cu Kα radiation) of BNT–$BT_{0.05}$ thin film derived from sol–gel and annealed at 700 °C, 1 h, in air is shown in Fig. 1. It has been reported that pure BNT thin films can completely crystallize at 700 °C. According to Fig. 1, the thin film has a polycrystalline structure, without any preferred orientation. The film shows dominant rhombohedral phase [30] (*pattern:* 01-070-9850) and minor pyrochlore phase.

The existence of pyrochlore phase in the BNT thin films derived from sol–gel, was also reported by other authors [18,25,31]. The appearance of minor pyrochlore phase can be avoided by using an excess of volatile Na and Bi precursors [28] or by using an oxygen atmosphere for a complete pyrolyze, after each layer of coating [18]. The incomplete combustion and the partial volatilization of A-site element from BNT can generate oxygen vacancies due to the valence balance. The oxygen vacancies increase the leakage current for the ferroelectric thin films. Mercurio and Marchet [31], consider that the minor phase with cubic symmetry results from the amorphous phase during the crystallization process. Kim et al. [25] reported that it can be eliminated by annealing at temperatures higher than 1050 °C.

3.2. Microstructure

Fig. 2(a) and (b) presents SEM micrographs of the BNT–$BT_{0.05}$ thin films, and show the morphology and particle size of the films heated at 700 °C for 1 h, in air. As it can be seen from Fig. 2(a), most of the particles are agglomerated. The primary particle (individual particle) size is quite uniform, with an average particle size of about 35 nm. The aggregates of 100 nm average size are formed by sticking primary particles together through the HO groups which are present in the gel precursor even at high temperature (>500 °C). It can be observed that there are a few small intergrain pores on the surface of the BNT–$BT_{0.05}$ films, which might be caused by solvent evaporation and combustion of organic groups from the precursor gel during the pyrolysis process.

Fig. 2(b) shows the cross-section micrograph of the BNT–$BT_{0.05}$ thin films. It can be seen that the film has an uniform thickness,

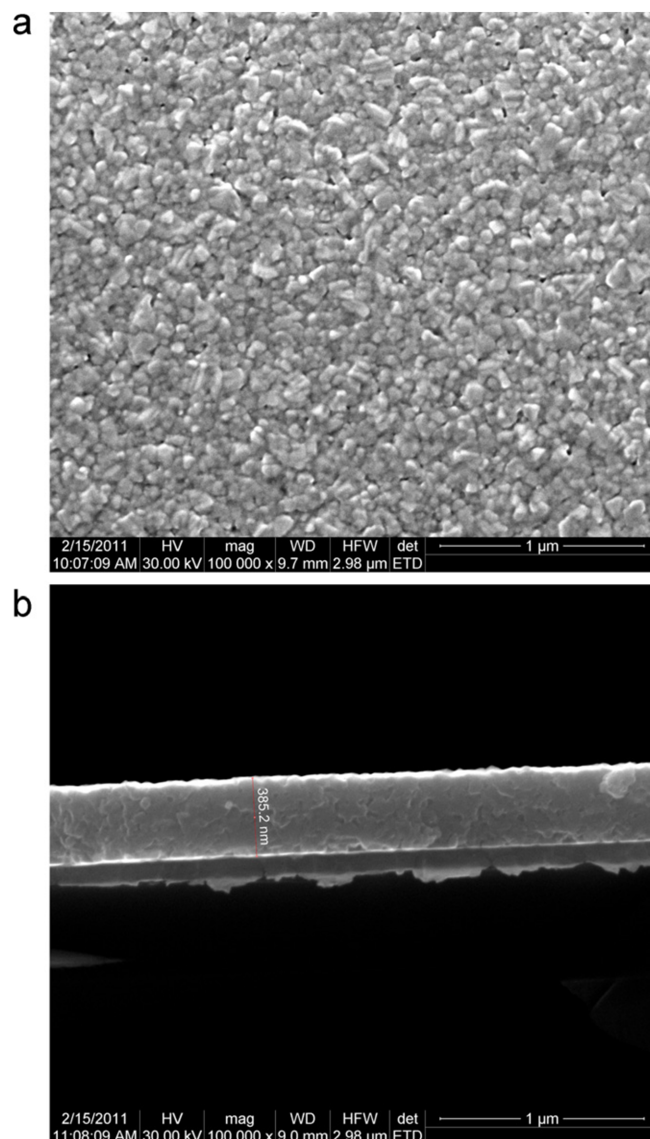

Fig. 2. SEM micrographs of the BNT–$BT_{0.05}$ thin films heated at 700 °C: (a) plan-view image and (b) cross-section image.

of about 385 nm. The BNT–$BT_{0.05}$ film exhibits a relatively dense grained structure (Fig. 2(b)).

Cross-section TEM samples were prepared by mechanically polishing using a tripod polisher for creating wedge-shaped specimens, with final stages of polishing performed on a 1 μm diamond lapping sheet. The specimens were then ion milled to electron transparency, at room temperature, using 4.5 kV argon ions incident at 5° (using double beam modulation).

The TEM and HR-TEM micrographs and SAED pattern of NBT–$BT_{0.05}$ thin film heated at 700 °C are shown in Fig. 3(a–c).

The TEM bright field image reveals that the film is composed of polyhedral shaped particles, with an average grain size of approximately 35 nm (Fig. 3(a)). The HR-TEM image (Fig. 3(b)) shows the lattice fringes of a polycrystalline nanoparticle with d = 3.90, 2.76 and 1.945 Å, corresponding to the (1 0 1), (0 1 2) and (2 0 2) crystallographic planes of the rhombohedral phase of $Na_{0.5}Bi_{0.5}TiO_3$. The regular succession of the atomic planes indicates that the nanocrystallites are structurally uniform. Both HR-TEM image and SAED pattern of NBT–$BT_{0.05}$ thin film indicate a rhombohedral $Na_{0.5}Bi_{0.5}TiO_3$ crystallographic phase, in good agreement with XRD analysis (Fig. 1).

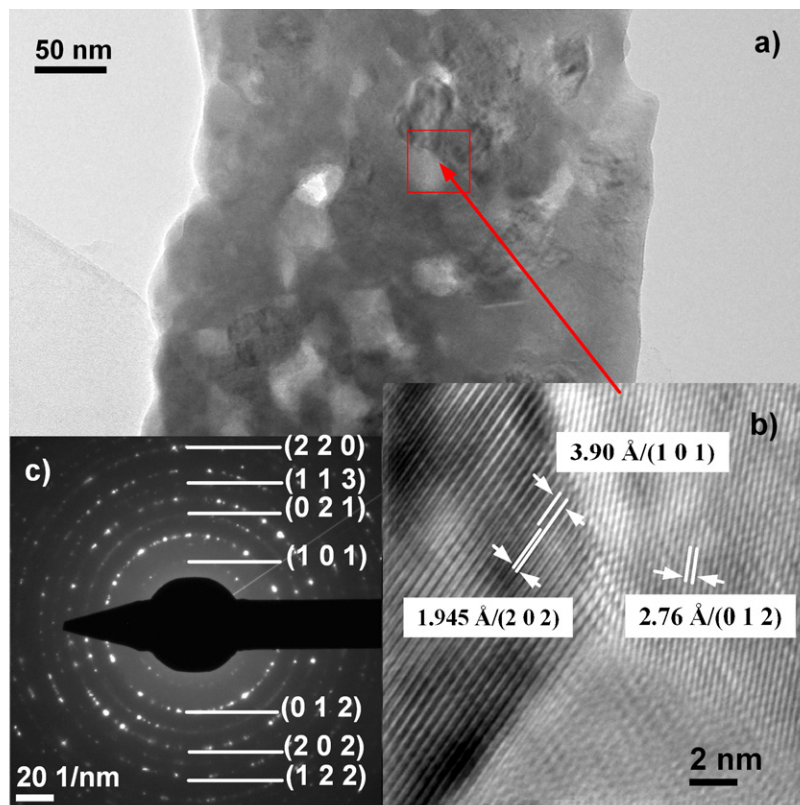

Fig. 3. Cross-sectional TEM images of the BNT–$BT_{0.05}$ thin film (a), corresponding HR-TEM of nanocrystals (b) and SAED image (c).

3.3. Dielectric and piezoelectric characterization

Fig. 4(a–c) shows the AFM, PFM phase and amplitude images of the BNT–$BT_{0.05}$ thin film. From the AFM image displayed in Fig. 4(a), it is possible to obtain the root mean square roughness (RMS) of the surface; a value of 4.52 nm was found. The RMS value of the film surface indicates a smooth morphology. The growth mechanism should be in a diffusion-limited mode in which a slow growth rate and a smooth surface would be expected to occur.

Fig. 4(b) and (c) presents the typical piezoresponse images, simultaneously obtained with the topography image (Fig. 4(a)), while Fig. 4(d) and (e) shows the line profile analysis of the morphology (d) and of the piezoresponse signal (e).

The strong and clear contrast of PFM domains indicates upward and downward polarized nanoregions, randomly distributed in BNT–$BT_{0.05}$ film at room temperature. From the cross-section analysis, which simultaneously investigates the surface morphology (grain size) (Fig. 4(d)) and domain populations (domain size and response signal) (Fig. 4(e)), one can see that a majority of the domains have dimensions smaller than the grain size, suggesting that the grains have a ferroelectric multidomain structure.

Fig. 5 (up) and (down) reveals the typical remnant piezoresponse amplitude and phase measurements, respectively, recorded as a function of applied dc voltage.

The polarization switching and hysteresis show clearly that the as-deposited BNT–$BT_{0.05}$ thin film is ferroelectric at nanoscale level. It can be observed that the hysteresis loop is shifted toward a positive voltage, indicating a built-in electric field. Local piezoresponse amplitude is given in arbitrary units as the PFM calibration has not been performed.

The ferroelectric properties of the BNT–$BT_{0.05}$ film with top and bottom Pt electrodes were investigated by performing hysteresis measurements at room temperature. Fig. 6 proves that, indeed, recorded hysteresis cycle is due to the ferroelectricity of BNT–$BT_{0.05}$ layer and there is no extrinsic phenomena artifact. The P–E loops are not fully saturated due to the oxygen vacancies that result in higher leakage current under high electric field. These P–E loops are consistent with the P–E loops previously reported [15,23,29]. The values of the remanent polarization $2P_r$ (5 $\mu C/cm^2$) and coercive field E_c (90 kV/cm) are higher than that of BNT–$BT_{0.11}$ film prepared in the same conditions [29], but smaller than that of the films deposited by other methods [23,32]. Note that the polarization values do not depend on frequency, which is normal for a hysteresis curve of ferroelectric dipole produced by the reversal. Only the contribution of leakage current depends on the frequency, being higher in lower frequencies. Dc leakage current does not depend on frequency, but integrated task during the measurement depends on the period (the period is equal to the inverse frequency) of AC voltage signal used to record the hysteresis cycle.

The voltage dependence of the dielectric constant, calculated from the capacitance measured at 100 kHz and 300 K, is shown in Fig. 7. Dielectric constant exhibits a significant change with the applied voltage. The dielectric constant and dielectric loss vs. applied voltage plots appear approximately symmetric, with a hysteresis behavior typical for ferroelectric capacitors. The maximum dielectric constant measured at zero bias voltage is about 210; this value is lower than obtained for BNT–$BT_{0.08}$ film [32], but higher than that of BNT–$BT_{0.11}$ thin film [29]. The results on BNT–$BT_{0.08}$ thin films confirm that the BNT–BT bulk and thin film with a composition near the morphotropic phase boundary (MPB) (x = 0.06–0.08) show best ferroelectric properties [12,13,33,34].

The relation between leakage current density and applied voltage at room temperature is sown in Fig. 8. The observed J has a value of about 3×10^{-5} A/cm^2 at an applied voltage about 8 V. Low leakage indicates high electric resistivity, as well as dense and good microstructure in the films, as shown in TEM image.

The asymmetry suggests that the structure is not perfectly symmetrical. We mention that although the electrodes are of the

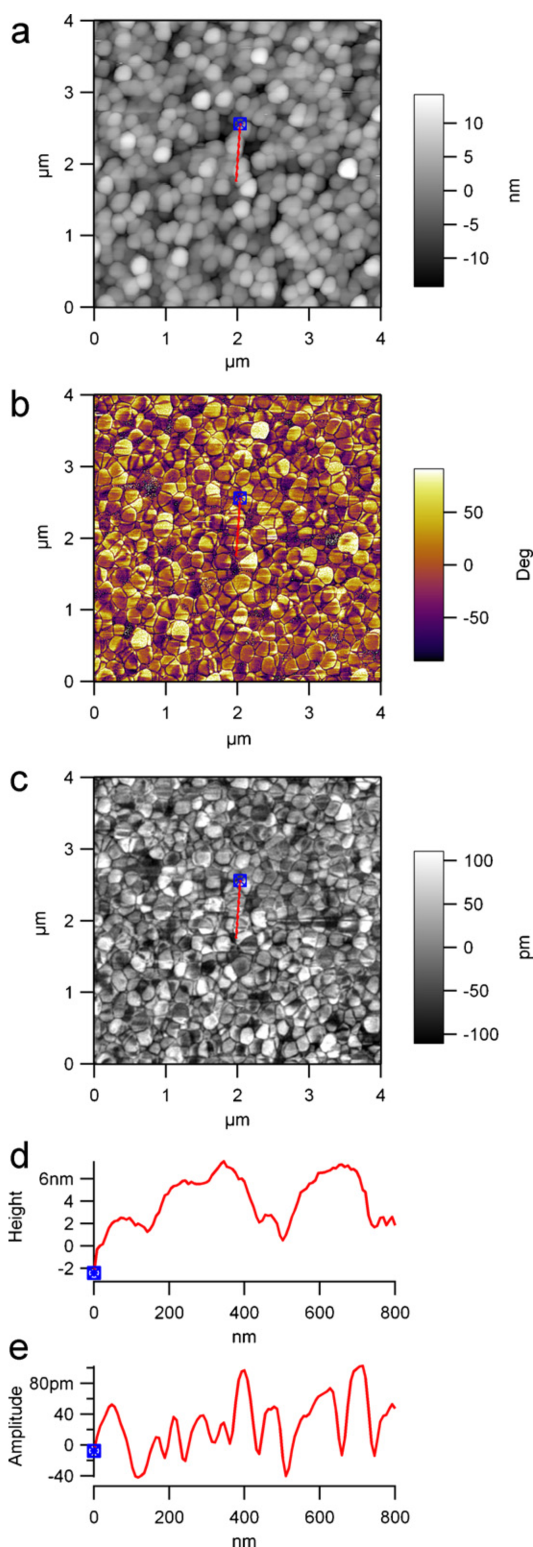

Fig. 4. Morphology image (a), phase (b) and amplitude (c) PFM images, line profile analysis of the morphology (d) and of the piezoresponse signal (e) of BNT–$BT_{0.05}$ thin films.

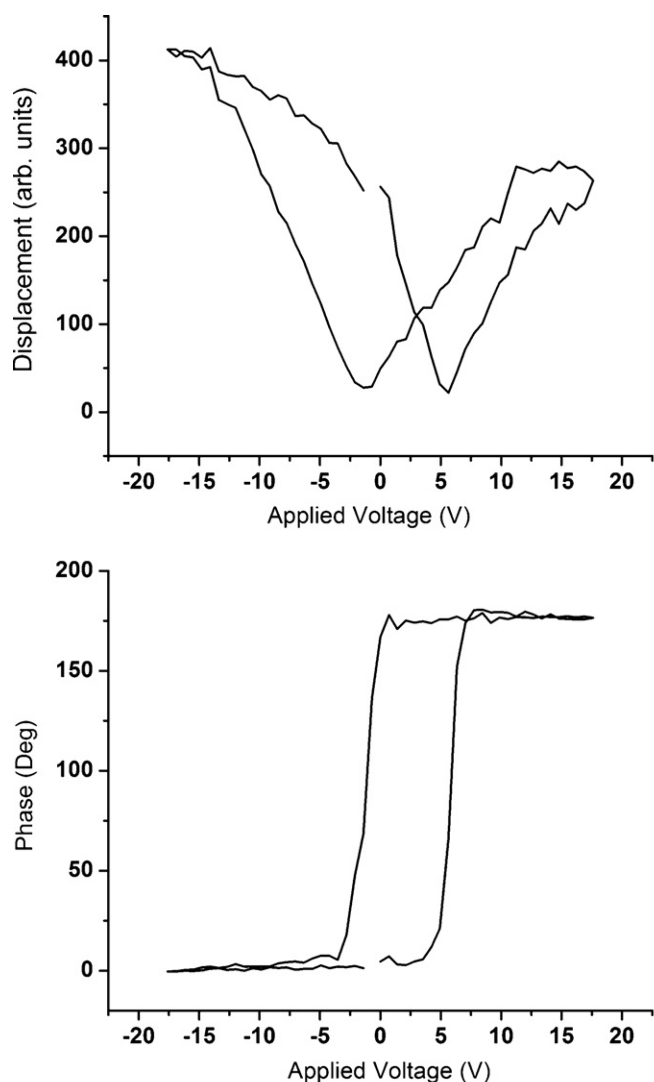

Fig. 5. Local PFM hysteresis loops measured on BNT–$BT_{0.05}$ thin film (up, amplitude signal; down, phase signal).

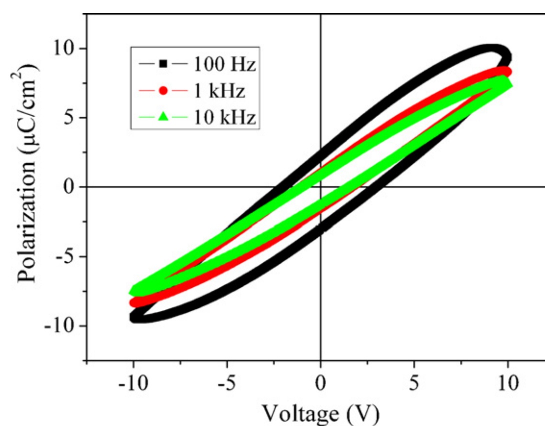

Fig. 6. *P–E* hysteresis loop of the BNT–$BT_{0.05}$ thin film under various electrical fields.

same metal (Pt), Pt–BNT–$BT_{0.05}$ interface, the two are not perfectly equivalent. The bottom interface was obtained by depositing and crystallizing BNT–$BT_{0.05}$ on Pt substrate, while the top interface was achieved by depositing Pt on BNT–$BT_{0.05}$ coating in RF. Even if the heat treatment is performed after the deposition of Pt top contact, the two interfaces remain different. All these differences can lead to different densities of interface states, with direct consequences on the electrical properties.

This study on BNT–$BT_{0.05}$ thin films will continue with the analysis of the electrode type influence on the electrical properties, as well as on the phenomena at the thin film/electrode interface.

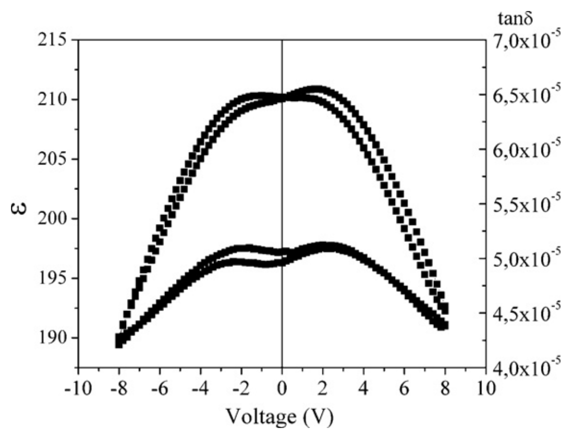

Fig. 7. The voltage dependence of dielectric constant (up) and dielectric loss (down) of the BNT–$BT_{0.05}$ thin film.

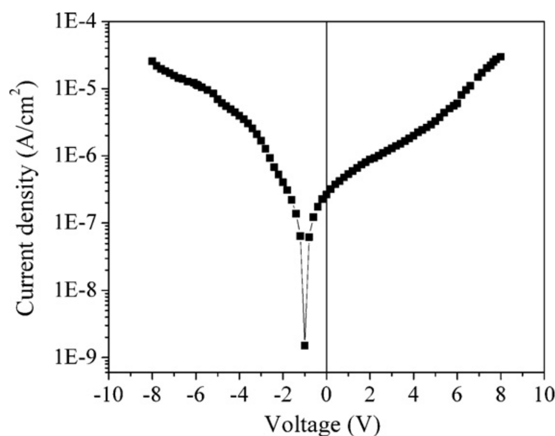

Fig. 8. Current density as a function of electric field for the Pt/BNT–$BT_{0.05}$/Pt thin film capacitor at room temperature.

4. Conclusions

In this paper, we have optimized the sol–gel/spin-coating process in order to prepare BNT–$NT_{0.05}$ thin films on Pt/TiO_2/SiO_2/Si substrates. The as-obtained films have a smooth surface and uniform grains of nano-scale size. The grains show a ferroelectric multidomain structure. It was found that in the case of 5% BT concentration, BNT–$BT_{0.05}$ thin film has a dielectric constant lower than that obtained for BNT–$BT_{0.08}$, but higher than that of BNT–$BT_{0.11}$ thin films, prepared in the same conditions.

Acknowledgement

The authors gratefully acknowledge the Romanian Research Ministry PNCDI II, Contract nr. 72-153/2008, for financial support.

References

[1] X. Jiang, M. Lin, N. Tu, C. Chen, S. Zhou, H. Zhan, J. Alloys Compd. 509 (2011) 9346–9350.
[2] A. Chaouchi, S. Kennour, S. d'Astorg, M. Rguiti, C. Courtois, S. Marinel, M. Aliouat, J. Alloys Compd. 509 (2011) 9138–9143.
[3] K.S. Rao, B. Tilak, K.C.V. Rajulu, A. Swathi, H. Workineh, J. Alloys Compd. 509 (2011) 7121–7129.
[4] H. Ni, L. Luo, W. Li, Y. Zhu, H. Luo, J. Alloys Compd. 509 (2011) 3958–3962.
[5] P. Fu, Z. Xu, R. Chu, W. Li, Q. Xie, Y. Zhang, Q. Chen, J. Alloys Compd. 508 (2010) 546–553.
[6] K.C. Singh, C. Jiten, R. Laishram, O.P. Thakur, D.K. Bhattacharya, J. Alloys Compd. 496 (2010) 717–722.
[7] H. Zhang, S. Jiang, K. Kajiyoshi, J. Alloys Compd. 495 (2010) 173–180.
[8] M. Abazari, A. Safari, S.S.N. Bharadwaja, S. Trolier-McKinstr, Appl. Phys. Lett. 96 (2010) 082903–082905.
[9] C.Y. Kim, T. Sekino, K. Niihara, J. Sol–Gel Sci. Technol. 55 (2010) 306–310.
[10] Q. Xu, X.L. Chen, W. Chen, B.H. Kim, S.L. Xu, M. Chen, J. Electroceram. 21 (2008) 617–620.
[11] Y.M. Chiang, G.W. Farrey, A.N. Soukhojak, Appl. Phys. Lett. 73 (1998) 3683–3685.
[12] T. Takenaka, K.I. Maruyama, K. Sakata, Jpn. J. Appl. Phys. 30 (1991) 2236–2239.
[13] B.J. Chu, D.R. Chen, G.R. Li, Q.R. Yin, J. Eur. Ceram. Soc. 22 (2002) 2115–2121.
[14] Q. Xu, S. Chen, W. Chen, S. Wu, J. Lee, J. Zhou, H. Sun, Y. Li, J. Alloys Compd. 381 (2004) 221–225.
[15] Y. Guo, D. Akai, K. Sawada, M. Ishida, Solid State Sci. 10 (2008) 928–933.
[16] H.W. Cheng, X.J. Zhang, S.T. Zhang, Y. Feng, Y.F. Chen, Z.G. Liu, G.X. Cheng, Appl. Phys. Lett. 85 (2004) 2319–2321.
[17] N. Scarisoreanu, F. Cracium, V. Ion, S. Birjega, M. Dinescu, Appl. Surf. Sci. 254 (2007) 1292–1297.
[18] T. Yu, K.W. Kwok, H.L.W. Chan, Thin Solid Films 515 (2007) 3563–3566.
[19] C.J. Brinker, G.W. Sherer, Sol–Gel Science, Academic Press, San Diego, 1990.
[20] C.J. Brinker, A.J. Hurd, P.R. Schunk, C.S. Ashely, R.A. Cairncross, J. Samuel, K.S. Chen, C. Scotto, R.A. Schwartz, Sol–gel derived ceramic films-fundamentals and applications, in: K. Stern (Ed.), Metallurgical and Ceramic Protective Coatings, Chapman & Hall, London, 1996, pp. 112–151.
[21] T. Troczynski, Q. Yang, Process for Making Chemically Bonded Sol–Gel Ceramics, US Pat. No. 6,284,682, May 2001.
[22] T. Olding, M. Sayer, D. Barrow, Thin Solid Films 398–399 (2001) 581–586.
[23] D.Z. Zhang, X.J. Zheng, X. Feng, T. Zhang, J. Sun, S.H. Dai, L.J. Gong, L. He, Z. Zhu, J. Huang, X. Xu, Y.Q. Gong, J. Alloys Compd. 504 (2010) 129–133.
[24] X.G. Tang, J. Wang, X.X. Wang, H.L.W. Chan, Chem. Mater. 16 (2004) 5293–5296.
[25] Y. Kim, T. Sekino, Y. Yamamoto, K. Niihara, J. Sol–Gel Sci. Technol. 33 (2005) 307–314.
[26] F. Remondiere, A. Wu, P.M. Vilarinho, Appl. Phys. Lett. 90 (2007) 152905–152907.
[27] F. Remondiere, B. Malic, M. Kosec, J.P. Mercurio, J. Sol–Gel Sci. Technol. 46 (2008) 117–125.
[28] D.A. Sanjose, R. Jimenez, I. Bretos, M.L. Calzada, J. Am. Ceram. Soc. 92 (2009) 2218–2225.
[29] M. Cernea, A.C. Galca, M.C. Cioangher, C. Dragoi, G. Ioncea, J. Mater. Sci. 46 (2011) 5621–5627.
[30] G.O. Jones, P.A. Thomas, Acta Crystallogr. B: Struct. Sci. 58 (2002) 168.
[31] J.P. Mercurio, P. Marchet, Integr. Ferroelectr. 61 (2004) 163–165.
[32] C. Dragoi, M. Cernea, L. Trupina, Appl. Surf. Sci. 257 (2011) 9600–9605.
[33] H. Wang, R. Zuo, X. Ji, Z. Xu, Mater. Des. 31 (2010) 4403–4407.
[34] W.W. Cao, L.E. Cross, Phys. Rev. B 47 (1993) 4825–4830.